Image Processing and Analysis of PET and Hybrid PET Imaging

12

Issam El Naqa

Contents

Abstract

PET imaging is a main diagnostic modality of different diseases including cancer. In the particular case of cancer, PET is widely used for staging of disease progression, identification of the treatment gross tumor volume, monitoring of disease, as well as prediction of outcomes and personalization of treatment regimens. Among the arsenal of different functional imaging modalities, PET has benefited from early adoption of quantitative image analysis starting from simple standard uptake value (SUV) normalization to more advanced extraction of complex imaging uptake patterns, thanks chiefly to the application of sophisticated image processing algorithms. In this chapter, we discuss the application of image processing techniques to PET imaging with special focus on the oncological radiotherapy domain starting from basic feature extraction to application in target definition using image segmentation/registration and more recent image-based outcome modeling in the radiomics field. We further extend the discussion into hybrid anatomical functional combinations of PET/CT and PET/MR multimodalities.

I. El Naqa, PhD, DABR
Department of Radiation Oncology, Physics Division, University of Michigan, 519 W. William St, Argus Bldg 1, Ann Arbor, MI 48103-4943, USA
e-mail: ielnaqa@med.umich.edu, https://sites.google.com/a/umich.edu/ielnaqa/

12.1 Introduction

Recent years have witnessed exponential growth in the use of imaging for diagnostic and therapeutic radiological purposes. In particular, positron emission tomography (PET) has been widely used in oncology for the purposes of diagnosis, grading, staging, and assessment of response. For instance, PET imaging with ^{18}F-FDG (fluoro-2-deoxy-d-glucose), a glucose metabolism analog, has been applied for diagnosis, staging, and treatment planning of lung cancer [1–10], head and neck cancer [11, 12], prostate cancer [13], cervical cancer [14, 15], colorectal cancer [16], lymphoma [17, 18], melanoma [19], and breast cancer [20–22]. Moreover, accumulating evidence supports that pretreatment or posttreatment FDG-PET uptake could be used as a prognostic factor for predicting outcomes [23–27]. For a review, see Chaps. 13 and 19.

Besides FDG-PET, other PET tracers have been also shown to be useful in interrogating tumor properties such as hypoxia by FMISO or Cu-ATSM and DNA synthesis and cell proliferation by FLT [28]. Interestingly, Denecke et al. compared CT, MRI, and FDG-PET in the prediction of outcomes to neoadjuvant radiochemotherapy in patients with locally advanced primary rectal cancer, demonstrating sensitivities of 100 % for FDG-PET, 54 % for CT, and 71 % for MRI and specificities of 60 % for FDG-PET, 80 % for CT, and 67 % for MRI [29]. Benz et al. showed that combined assessment of metabolic and volumetric changes predicts tumor response in patients with soft tissue sarcoma [30]. Similarly, Yang et al. showed that the combined evaluation of contrast-enhanced CT and FDG-PET/CT predicts the clinical outcomes in patients with aggressive non-Hodgkin's lymphoma [31]. Indeed, quantitative information from hybrid imaging modalities could be related to biological and clinical endpoints, a new emerging field referred to as "radiomics" [32, 33]. We were among the leading groups to demonstrate the potential of this new field to monitor and predict response to radiotherapy in head and neck [34], cervix [34, 35], and lung [36] cancers, in turn allowing for adapting and individualizing treatment regimens.

In this chapter, we discuss the application of advanced image processing techniques in PET imaging with specific focus on two major areas of better tumor target definition and image-based prediction of treatment outcomes.

12.2 Image Features from PET

A necessary prerequisite of image processing application in PET is the robust extraction of relevant imaging features, which could be used in varying applications. The features extracted from PET images could be divided into static (time-invariant) and dynamic (time-variant) features according to the acquisition protocol at the time of scanning and into pre- or intra-treatment features according to the scanning time point [37].

12.2.1 Static PET Features

(a) *Standard uptake value* (*SUV*) *descriptors*: SUV is a standard method in PET image quantitative analysis [38]. In this case, raw intensity values are converted into SUVs, and statistical descriptors such as maximum, minimum, mean, standard deviation (SD), and coefficient of variation (CV) are extracted.

(b) *Total lesion glycolysis* (*TLG*): This is defined as the product of volume and mean SUV [5, 30, 39].

(c) *Intensity-volume histogram* (*IVH*): This is analogous to the dose-volume histogram widely used in radiotherapy treatment planning in reducing complicated 3D data into a single easier to interpret curve. Each point on the IVH defines the absolute or relative volume of the structure that exceeds a variable intensity threshold as a percentage of the maximum intensity [34]. This method would allow for extracting several metrics from PET images for outcome analysis such as I_x (minimum intensity to x% highest intensity volume), V_x (percentage volume having at least x% intensity value), and descriptive statistics (mean, minimum, maximum, standard

deviation, etc.). We have reported the use of the IVH for predicting local control in lung cancer [36], where a combined metric from PET and CT image-based model provided a superior prediction power compared to commonly used dosimetric-based models of local treatment response.

(d) *Morphological features*: These are generally geometrical shape attributes such as eccentricity (a measure of non-circularity), which is useful for describing tumor growth directionality, and Euler number (the number of connected objects in a region minus the total number of holes in the objects) the solidity (this is a measurement of convexity), which may be a characteristic of benign lesions [40, 41]. An interesting demonstration of this principle is that a shape-based metric based on the deviation from an idealized ellipsoid structure (i.e., eccentricity) was found to have strong association with survival in patients with sarcoma [41, 42].

(e) *Texture features*: Texture in imaging refers to the relative distribution of intensity values within a given neighborhood. It integrates intensity with spatial information resulting in higher-order histograms when compared to common first-order intensity histograms. It should be emphasized that texture metrics are independent of tumor position, orientation, size, and brightness and take into account the local intensity spatial distribution [43, 44]. This is a crucial advantage over direct (first-order) histogram metrics (e.g., mean and standard deviation), which only measures intensity variability independent of the spatial distribution in the tumor microenvironment. Texture methods are broadly divided into three categories: statistical methods (e.g., high-order statistics, co-occurrence matrices, moment invariants), model-based methods (e.g., Markov random fields, Gabor filter, wavelet transform), and structural methods (e.g., topological descriptors, fractals) [45, 46]. Among these methods, statistical approaches based on the co-occurrence matrix and its variants such as the gray-level co-occurrence matrix (GLCM), neighborhood gray-tone difference matrix (NGTDM), run-length matrix (RLM), and gray-level size zone matrix (GLSZM) have been widely applied for characterizing FDG-PET heterogeneity [47].

Four commonly used features from the GLCM include energy, entropy, contrast, and homogeneity [44]. The NGTDM is thought to provide more humanlike perception of texture such as coarseness, contrast, busyness, and complexity. RLM and GLSZM emphasize regional effects. Textural map examples from multiple PET tracers are shown in Fig. 12.1.

These features were shown to predict response in cancers of the cervix [34], esophagus [48], head and neck [49], and lung cancer [50]. MaZda is a dedicated software for image feature analysis [51]. An example of PET different feature extraction from head and neck cancer is shown in Fig. 12.2.

12.2.2 Dynamic PET Features

These features are based on kinetic analysis using tissue compartment models and parameters related to transport and binding rates [52]. In the case of FDG, a three-compartment model could be used to depict the trapping of FDG-6-phosphate (FDG6P) in tumor [53, 54]. Using estimates from compartmental modeling, glucose metabolic uptake rate could be evaluated. The uptake rate and other compartment estimates themselves could form "parameter map" images, which previously described static features, and could be derived from as well (see Chap. 14).

Glucose metabolic rate was correlated with pathologic tumor control probability in lung cancer [55]. Thorwarth et al. published interesting data on the scatter of voxel-based measures of local perfusion and hypoxia in head and neck cancer [56, 57]. Tumors showing a wide spread in both showed less reoxygenation during a course of radiotherapy and had lower local control. A rather interesting approach to improve the robustness of such features is the use of advanced 4D iterative techniques; an example is given in Fig. 12.3. Further improvement could be achieved by utilizing multi-resolution transformations
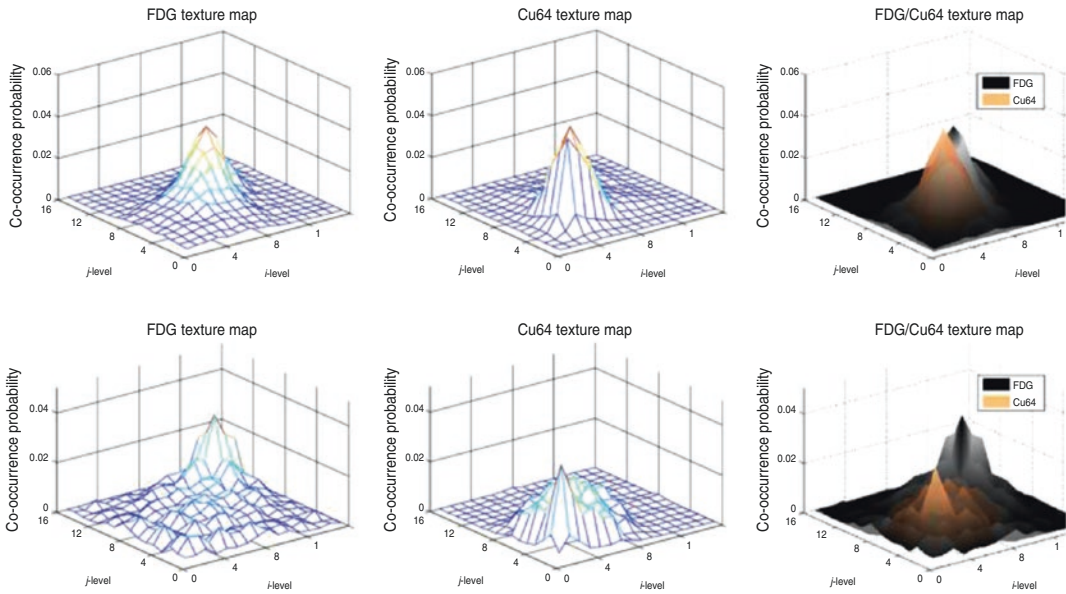
Fig. 12.1 The two rows, referring to an individual patient with primary cervical cancer, show texture maps for FDG (metabolic marker) and Cu-ATSM (hypoxia marker) alone and overlapping texture maps of the two markers [37]

(e.g., wavelet transform) to stabilize kinetic parameter estimates spatially [58].

12.3 Extension to PET/CT and PET/MR

Combining information from multiple modalities allows for better utilization of complementary features from different images. For instance, several studies have indicated that inter- and intra-observer variability of defining the tumor extent could be reduced by using PET/CT or PET/MR. Researchers in lung cancer reported reduced variability when using CT with PET for target definition [3, 10]. Furthermore, a study of fractionated stereotactic radiotherapy for meningioma patients demonstrated improved target definition by combining physiological information from PET, anatomical structure from CT, and soft tissue contrasts from MRI, resulting in alterations of the original contour definitions in 73 % of the cases [59]. However, this visual approach for integrating multimodality imaging information is prone to observer subjectivity and variations as contrasted to single image analysis as discussed later.

The PET imaging features presented as static metrics in Sect. 12.2.1 could be applied equally to PET/CT or PET/MR, where instead of SUV, Hounsfield units are used in the case of CT, and T1w or T2w images, for instance, could be used in the case of MRI, for instance, using its weighted relaxation times or proton density pixel intensities. In the case of dynamic MRI acquisitions, the corresponding pharmacokinetic models would be applied to extract the parametric maps such as extended Tofts model [60], which is also a three-compartment model, and extracted parameters include the transfer constant (K_{trans}), the extravascular-extracellular volume fraction (ve), and the blood volume (bv).

However, among the most challenging issues in multimodality imaging is the fusion of multiple imaging data from different scanners. This is typically carried out through a geometric transformation, i.e., image registration. This could be solved greatly using integrated hardware systems such as PET/CT scanners or PET/MRI scanners; otherwise, software solutions need to be deployed. These software solutions could be divided into rigid or deformable registration techniques [61]. In
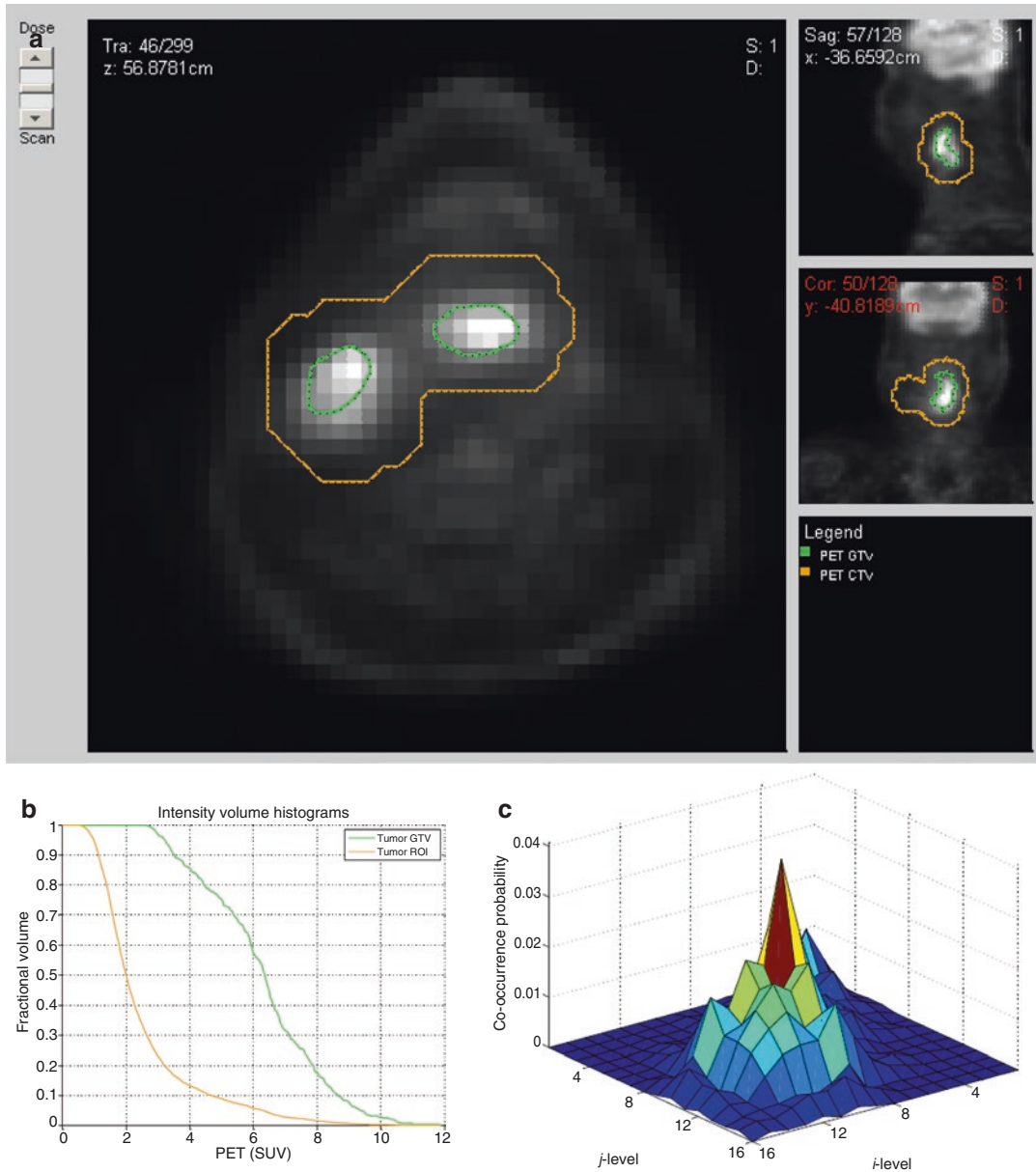
Fig. 12.2 A pretreatment PET scan of a head and neck cancer case of a patient who died from disease after radiotherapy treatment. (**a**) The head and neck tumor region of interest (*brown*) and the gross tumor volume (GTV) (*green*) were outlined by the physician. (**b**) An IVH plot, where I_x and V_x parameters are derived. (**c**) A texture map plot of the GTV heterogeneity through intensity spatial mapping

our previous work, we have developed several tools for this purpose such as MIASYS [62] and DIRART [63]. https://sites.google.com/a/umich.edu/ielnaqa/home/software-tools.

MIASYS is a dedicated open-source software tool developed in MATLAB for multimodality image analysis. The software tool aims to provide a comprehensive solution for 3D image segmentation by integrating automatic algorithms, manual contouring methods, image pre-processing filters, post-processing procedures, user-interactive features, and evaluation metrics.
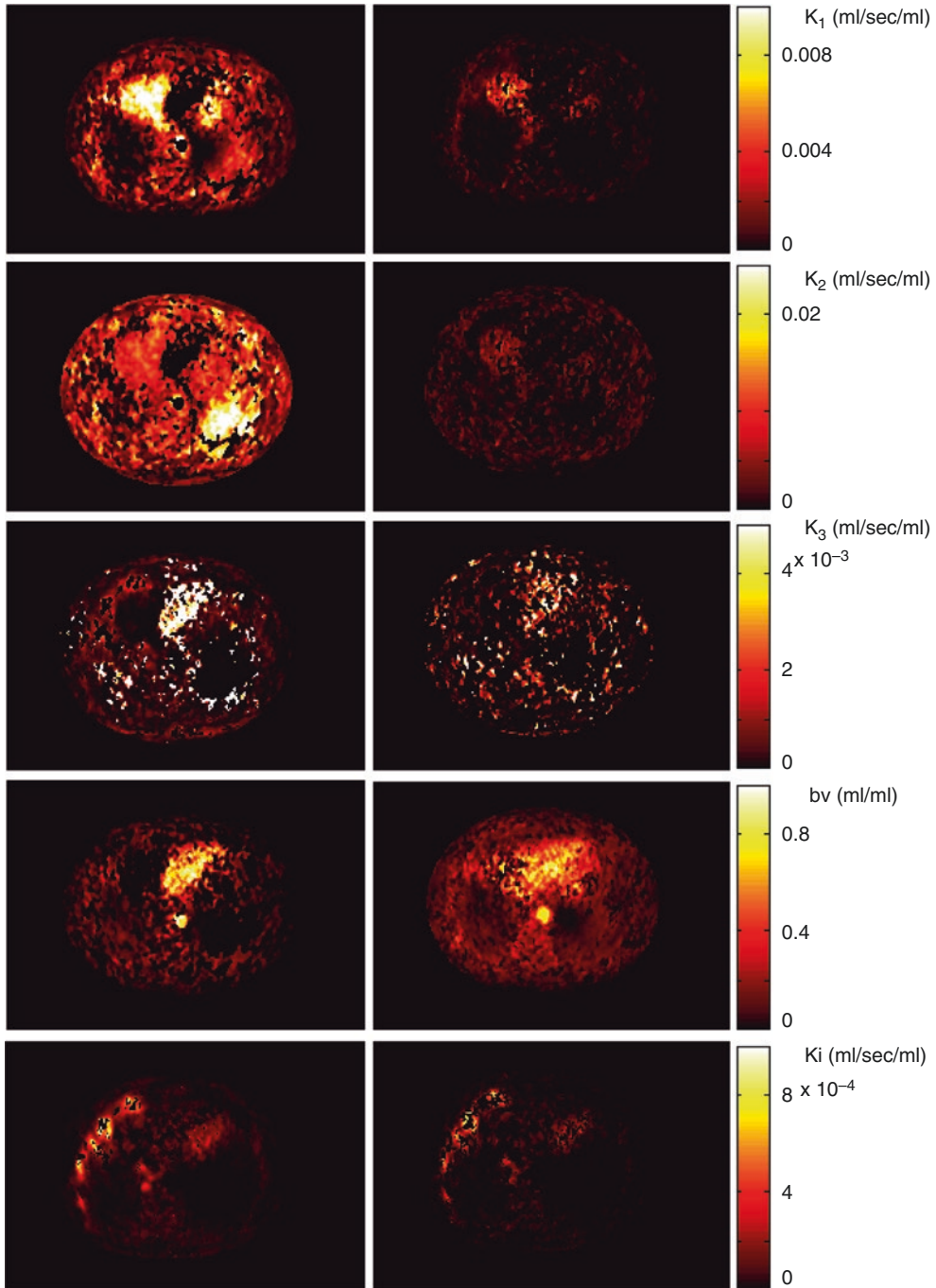
Fig. 12.3 An abdominal dynamic FDG-PET/CT kinetic analysis. The figure shows the three-compartment parameter map (K_1, k_2, k_3) model assuming irreversible kinetics ($k_4 = 0$), blood volume component ($bv = K_1/k_2$), and K_{FDG} net influx rate constant (Ki). In this case, the parameters were obtained using a 4D iterative technique (compared with simple differential methods) by estimation directly from the sinogram domain

The implemented methods include multiple image thresholding, clustering based on K-means and fuzzy C-means (FCM), and active contours based on snakes and level sets. Image registration is achieved via manual and automated rigid methods [62].

DIRART is also an open-source software implemented in MATLAB to support deformable image registration (DIR) for adaptive radiotherapy applications. Image registration in this regard computes voxel mapping between two image sets and is formulated as an optimization problem in which the solution is found by maximizing a similarity metric between the two images (e.g., mutual information). DIRART contains 20+ deformable image registration (DIR) algorithms including 12 different optical flow algorithms, different demon algorithms, and four level set algorithms. It also supports interface to ITK so that ITK DIR algorithms can be called from within DIRART. Currently five ITK DIR algorithms are supported, including demon algorithms and B-spline algorithms. In addition, the newer inverse consistency algorithms to provide consistent displacement vector field (DVF) in both forward and backward directions are implemented [63].

12.4   Application of PET in Radiotherapy

In the following, we discuss the application of PET to radiotherapy with focus on two cases, contouring of tumor/organs at risk in treatment planning and outcome prediction for clinical decision-making using radiomics.

12.4.1 Biological Target Definition Using PET

Medical image segmentation is a process to separate structures of interest in an image from its background or other neighboring structures. It is a necessary prerequisite step for many medical imaging applications in radiology and radiation therapy. These applications may include automatic

organ delineation, quantitative tissue classification, surface extraction, visualization and image registration, etc. [64, 65]. For instance, Pham and coworkers divided segmentation algorithms into eight different categories: thresholding, region growing, classifiers, clustering, Markov random field models, artificial neural networks, deformable models, and atlas-guided approaches. In our work on PET-guided treatment planning in radiotherapy, we presented a comparative survey of the current methods applied for tumor segmentation [66, 67]; an example in head and neck cancer using different segmentation algorithms is presented in Fig. 12.4.

There are several commercial and academic software tools that support different segmentation algorithms. In general, commercial software packages have better implementations with a user-friendly interface for manual and semiautomatic segmentation methods, but often lag behind the latest development in the field. In contrast, academic software packages, such as ITK [68], BioImage Suite [69], MIPAV [70], ImageJ [71], and 3D slicer [72], may tend to be oriented toward single-modality applications and less friendly in handling multimodality images as proposed here.

Most automatic algorithms attempt to utilize image intensity variations or image gradient information. However, for low-contrast images, many of these algorithms tend to provide suboptimal solutions that are not clinically acceptable. For such cases, it has been demonstrated that if multiple images are available for the same object (the same image modality or different image modalities), all the available complementary information can be fed into the segmentation algorithms to define the so-called biophysical target [73]. Thus, the segmentation algorithms would benefit from the complementary information from different images, and consequently the accuracy of the final segmentation results could be improved. Similar approaches have been applied for detecting blood-wall interface of heart ventricles from CT, MRI, and ultrasound images using a snake deformable model [74], for classifying coronary artery plaque composition from multiple contrast MR images using K-means
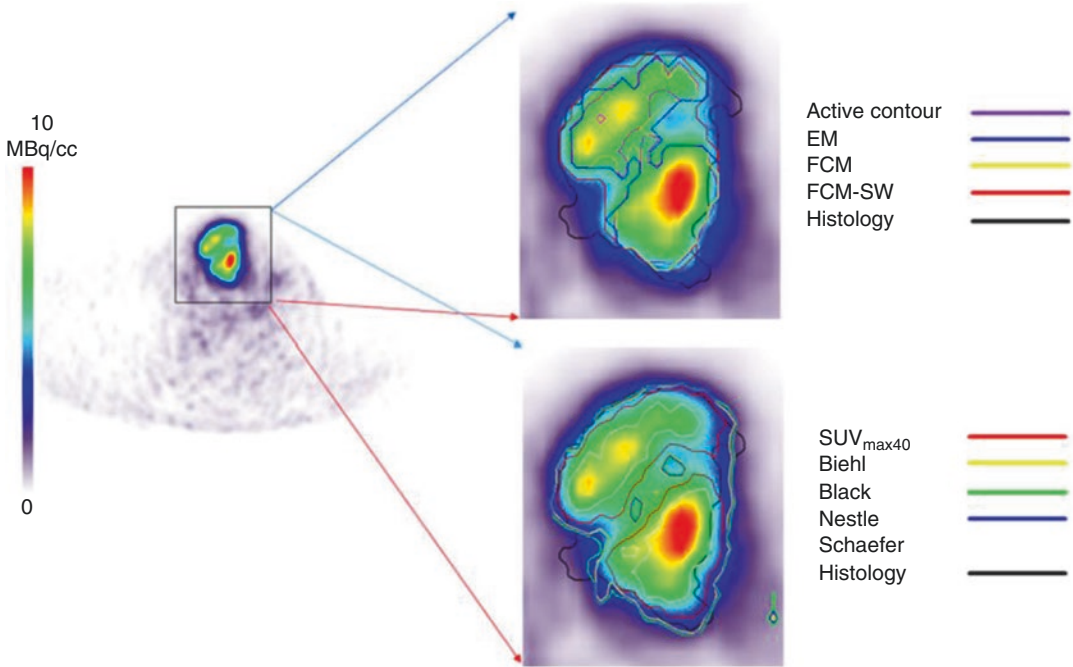
Fig. 12.4 Example of different PET segmentation methods of head and neck cancer. The methods include 40 % of SUV_{max} (SUV_{max40}) and the methods of Nestle, Black, Biehl, and Schaefer. This is in addition to the level set technique (active contour), the stochastic EM approach (EM), the FCM algorithm (FCM), and the FCM-SW variant of the FCM algorithm (FCM-SW). The 3D contour defined on the macroscopic tumor specimen is used as the reference for assessing the performance of the different segmentation techniques (From Zaidi et al. [66])

clustering algorithm [75], and for defining tumor target volumes using PET/CT/MR images for radiotherapy treatment planning by using a multivalued deformable level set approach as in our previous work. Mathematically, such an approach is a framework that could be thought of as a mapping from the imaging space to the "perception" space as identified by the radiologists [73]:

$$\text{Biophysical target} = f\left(\text{CT, PET, MRI}, ..., \lambda\right) \quad (12.1)$$

where $f(\cdot)$ is the mapping function from the different imaging modalities to the target space parameterized by λ, which represents users' defined set of parameters representing the prior knowledge. This framework is highlighted in Fig. 12.5.

The robust image segmentations methods are based on deformable models, which are geometric representations of curves or surfaces that are defined explicitly or implicitly in the imaging

Fig. 12.5 Biophysical target as generated from multimodality imaging by combining anatomical and functional information

domain. These models move under the influence of internal forces (contour curvature) and external forces (image boundary constraints) [76, 77]. The

level set is a state-of-the-art variational method for shape recovery [76, 78–80]. They were originally developed in curve evolution theory to overcome the limitations encountered in parametric deformable models (e.g., snakes [81]) such as initialization requirement, generalization to 3D, and topological adaptation such as splitting or merging of model parts. Our generalization to multimodality imaging is based on redefining the concept of a boundary as a logical or "best" combination of multiple images by learning and incorporating expert's knowledge on subregional or even voxel levels. An example showing combination of PET/CT in lung cancer is shown in Fig. 12.6 using a multivalued level set algorithm [73].

In another example the PET/CT images were taken from patients with cervix cancer. The PET image was sharpened using a deconvolution approach [82]. The 40 % maximum SUV (standard uptake value) thresholding is adopted in many institutes to estimate gross tumor volume for cervix cancer patients due to the high target to background ratio of these tumors in PET and the difficulty to distinguish their boundary in CT. In Fig. 12.7, the active contour algorithm is initialized with a circle (in white) of 15.9 mm diameter around the PET lesion. The evolved contour took ten iterations (in blue) and the final estimated contours (in thick black) are shown. The algorithm converged in just 30 iterations. This fast convergence could be attributed in part to the almost spherical shape of the tumor and the sharpness of the gradient. It is noticed that the results of the algorithm match the PET ground truth (99 %) as delineated by an experienced nuclear medicine radiologist. Hence, the delineation results were explained mainly by PET in this case, although information from CT could still be used to steer the algorithm, if desired.

12.4.2 PET Radiomics

The extraction of quantitative information from imaging modalities and relating information to biological and clinical endpoints is a new emerging field referred to as "radiomics" [32, 33]. Traditionally, quantitative analysis of FDG-PET or other PET tracer uptake is conducted based on observed changes in the standard uptake value (SUV). For instance, decrease in SUV postirradiation has been associated with better outcomes in lung cancer [83, 84]. However, SUV measurements themselves are potentially pruned to errors due to the initial FDG uptake kinetics and radiotracer distribution, which are dependent on the initial dose and the elapsing time between injection and image acquisition. In addition, some commonly reported SUV measurements might be sensitive to changes in tumor volume definition (e.g., mean SUV). These factors and others might make such approach subject to significant intra- and inter-observer variability [25, 26, 34].

Radiomics consist of two main steps, extraction of static and dynamic features as discussed in Sect. 17.3 and outcome modeling as presented in the following. Outcomes in oncology and particularly in radiation oncology are characterized by tumor control probability (TCP) and the surrounding normal tissue complication probability (NTCP) [85, 86]. A detailed review of outcome modeling in radiotherapy is presented in our previous work [87]. DREES is a dedicated software tool for modeling of radiotherapy response [88]. In the context of image-based treatment outcome modeling, the observed outcome (e.g., TCP or NTCP) is considered to be adequately captured by extracted image features [34, 89]. We will highlight this approach using classical logistic regression.

Logistic modeling is a common tool for multimetric modeling. In our previous work [90, 91], a logit transformation was used:

$$f\left(\mathbf{x}_i\right) = \frac{e^{g(\mathbf{x}_i)}}{1 + e^{g(\mathbf{x}_i)}}, \quad i = 1, \ldots, n, \quad (12.2)$$

where n is the number of cases (patients) and $\mathbf{x}_i$ is a vector of the input variable values (i.e., image features) used to predict $f(\mathbf{x}_i)$ for outcome y_i (i.e., TCP or NTCP) of the i_{th} patient
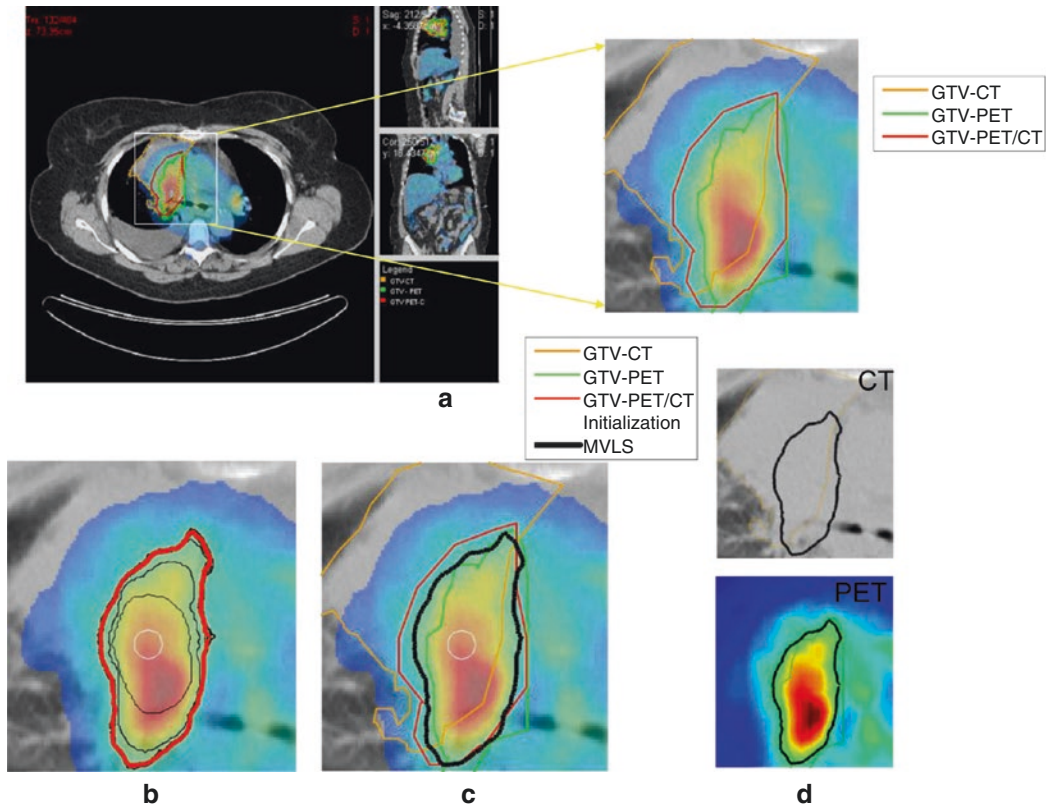
Fig. 12.6 Joint estimation of lung PET/CT target/disease volume. (**a**) A fused PET/CT displayed in CERR with manual contouring shown of the subject's right gross tumor volume. The contouring was performed separately for CT (*in orange*), PET (*in green*), and fused PET/CT (*in red*) images. (**b**) The MVLS algorithm was initialized with a circle (*in white*) of 9.8 mm diameter, an evolved contour in steps of ten iterations (*in black*), and the final estimated contour (*in thick red*). The algorithm converged in 120 iterations in few seconds. The PET/CT ratio weighting was selected as 1:1.65. (**c**) MVLS results are shown along with manual contour results on the fused PET/CT. Note the agreement of the fused PET/CT manual contour and MVLS (dice=0.87). (**d**) MVLS contour superimposed on CT (*top*) and PET (*bottom*) separately

$$g\left(\mathbf{x}_i\right) = \beta_o + \sum_{j=1}^{d} \beta_j x_{ij}, \quad i = 1,\ldots,n, \ j = 1,\ldots,d,$$

(12.3)

where d is the number of model variables and the βs are the set of model coefficients determined by maximizing the probability that the data gave rise to the observations. Resampling methods such as cross validation and bootstrapping methods could be used to determine optimal model order and parameter selection as shown in Fig. 12.8 for PET/CT modeling of lung cancer [36]. Interestingly, a model of two parameters from PET and CT based on intensity-volume histograms provided the best fit to local control.

12.5 Current Issues and Future Directions

12.5.1 PET Image Characteristics

Generally speaking, PET images have lower resolution than CT or MRI in the order of 3–5 mm, which is further worsened under cardiac or respiratory motion conditions due to longer acquisition periods. Moreover, PET images are susceptible to limited photon count noise. Advances in hardware such as crystal detector technologies [92] and software such as image reconstruction techniques [93] are poised to improve PET image quality and their subsequent use. See Chaps. 8 and 11.
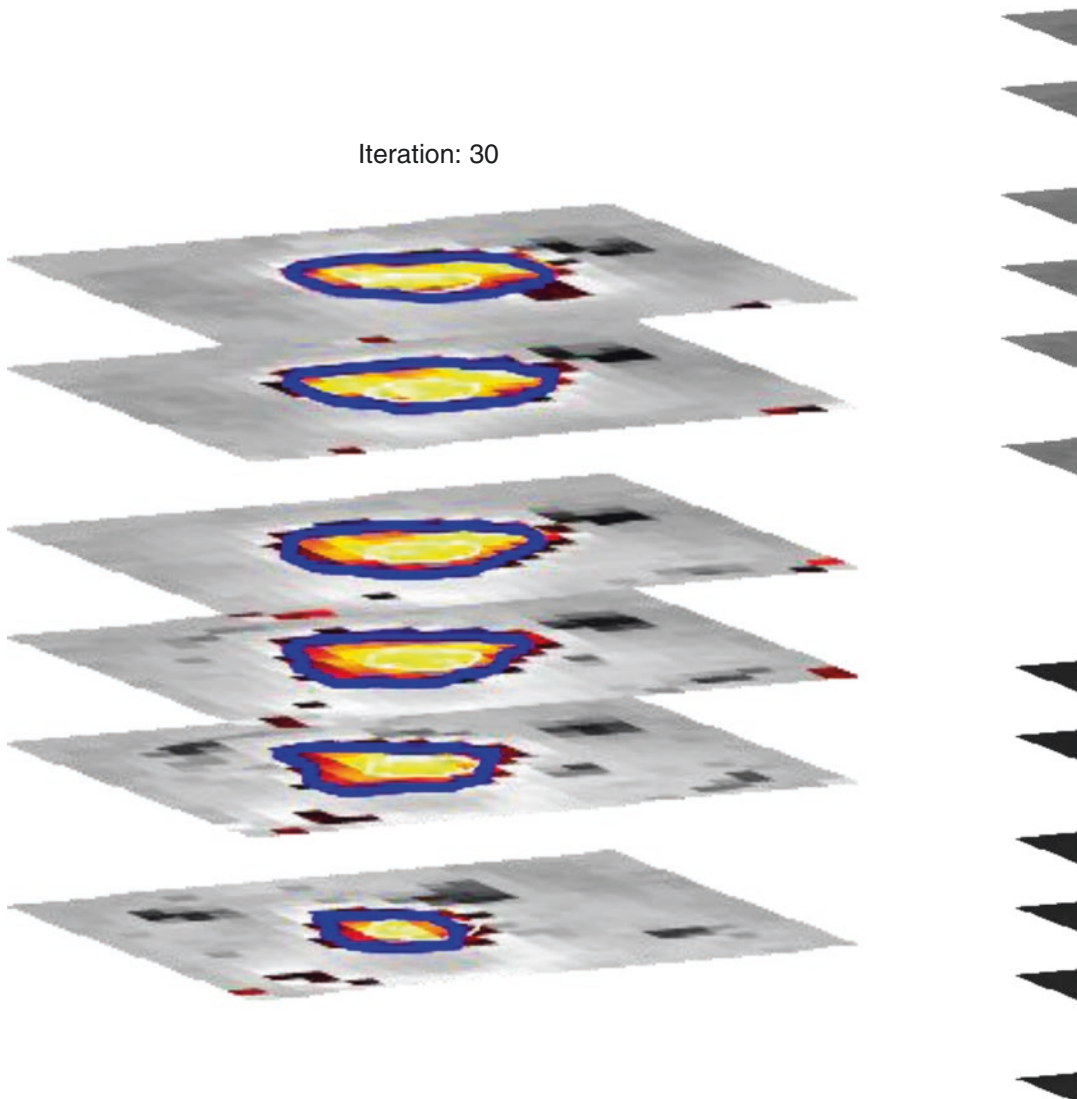
Iteration: 30

Fig. 12.7 A 3D generalization of multivalued level set (MVLS) algorithm in the case of PET/CT cervix. The MVLS algorithm is initialized with a sphere (*in white*) of 15.9 mm diameter, a curve evolution in steps of ten iterations (*in magenta*), and the final estimated contour (*in thick blue*). The algorithm converged in 30 iterations. MVLS estimated contour superimposed on CT. MVLS estimated contour superimposed on PET

12.5.2 Robustness and Stability of Extracted Image Features

It is well recognized that image acquisition protocols may impact the reproducibility of extracted features from PET images, which may consequently impact the robustness and stability of these features for image analysis. This includes static features such as SUV descriptors [94–96] and texture features [97, 98]. Interestingly, texture-based features were shown to have a reproducibility similar to or better than that of simple SUV descriptors [99]. Moreover, textural features from the GLCM seemed to exhibit lower variations than NGTDM features [97]. Other factors that may impact the stability of these features may include signal-to-noise ratio (SNR), partial volume effect, motion artifacts, parameter
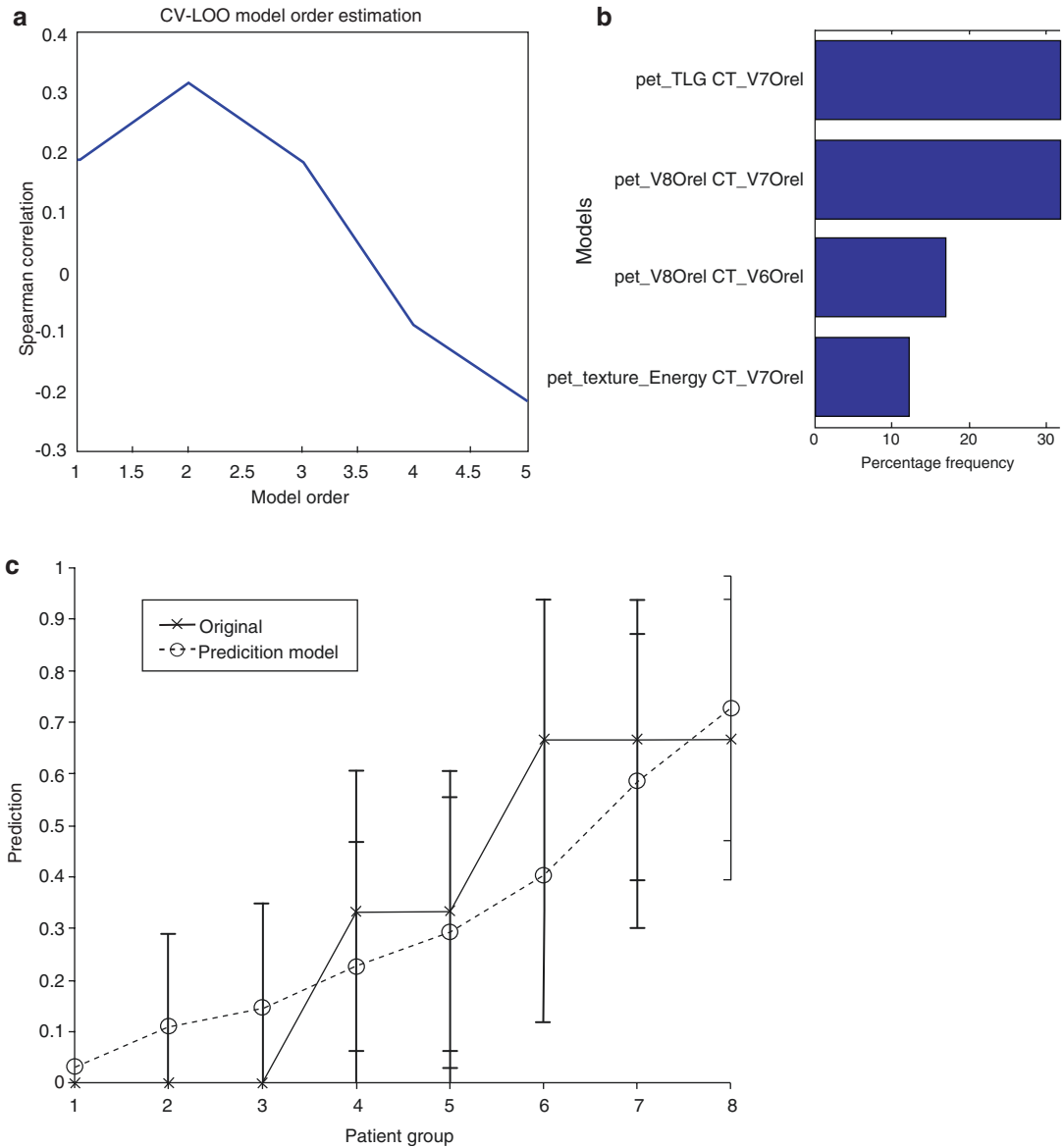
Fig. 12.8 Multi-metric modeling of local failure from PET/CT features. (**a**) Model-order selection using leave-one-out cross validation. (**b**) Most frequent model selection using bootstrap analysis where the *y*-axis represents the model selection frequency on resampled bootstrapped samples. (**c**) Plot of local failure probability as a function of patients binned into equal-size groups showing the model prediction of treatment failure risk and the original data (Reproduced with permission from Vaidya et al. [36])

settings, resampling size, and image quantization [34, 98]. Denoising methods for mitigation of noise in PET imaging follow their limited photon effects using traditional denoising filtering methods [66, 100] or more advanced methods based on combining wavelet and curvelet transform characteristics [101].

12.5.3 Improved PET-Based Outcome Models

In addition to using appropriate candidate image features for PET-based outcome modeling, "radiomics," a main weakness in using classical logistic regression formalism is that the model's

capacity to follow details of the data trends is limited. In addition, Eq. (12.3) requires the user's feedback to determine whether interaction terms or higher-order terms should be added, making it a trial-and-error process. A solution to ameliorate this problem is offered by applying machine learning methods [102].

A class of machine learning methods that is particularly powerful, and which we propose to use for image-based outcome prediction, includes so-called kernel-based methods and their most prominent subtype, support vector machines (SVMs). These methods have been applied successfully in many diverse areas including outcome prediction [103–107]. Learning is defined in this context as estimating dependencies from data [108]. In the example of outcome prediction (i.e., discrimination between patients who are at low risk versus patients who are at high risk of local failure), the main function of the kernel-based technique would be to separate these two classes with "hyperplanes" that maximize the margin (separation) between the classes in the nonlinear feature space. The objective here is to minimize the bounds on the generalization error of a model on unseen data before rather than minimizing the mean-square error over the training dataset itself (data fitting). Note that the kernel in these cases acts as a similarity function between sample points in the feature space. Moreover, kernels enjoy closure properties, i.e., one can create admissible composite kernels by weighted addition and multiplication of elementary kernels. This flexibility allows for the construction of a neural network by using a combination of sigmoidal kernels. Alternatively, one could choose a logistic regression equivalent kernel by proper choice of the objective function itself.

Evaluation of radiomics in clinical trials is still in its infancy. According to the website clinicaltrials.gov, a registered trial for "Radiomics: A Study of Outcome in Lung Cancer" between the Maastro Clinic in the Netherlands, Moffitt Cancer Center and Research Institute from Florida, USA, and Gemelli Hospital from Rome, Italy, is reported. Another trial on "Radiomics Prediction of Long Term Survival and Local

Failure After Stereotactic Radiotherapy for Brain Metastases" by the Maastro Clinic has been recently opened.

Conclusions

Image processing constitutes an indispensible set of tools for analyzing and extracting valuable information from PET images. We presented in this chapter an overview of different features that could be extracted from PET images for different applications including contouring and response prediction. We have shown that incorporation of different anatomical information from CT and MRI into PET is feasible and could yield better results. However, there are challenges still in the use of PET, some are related to inherited image quality, and others are related to standardization of image acquisition protocols and reconstruction algorithms. Nevertheless, advances in hardware and software technologies will further facilitate wider application of advanced image processing techniques to PET and hybrid imaging to achieve better clinical results. In particular, the synergy between image analysis and machine learning could provide powerful tools to strengthen and further the utilization of PET in clinical practice.

References

1. Verhagen AF, Bootsma GP, Tjan-Heijnen VC, van der Wilt GJ, Cox AL, Brouwer MH, et al. FDG-PET in staging lung cancer: how does it change the algorithm? Lung Cancer. 2004;44:175–81.
2. Bradley J, Thorstad WL, Mutic S, Miller TR, Dehdashti F, Siegel BA, et al. Impact of FDG-PET on radiation therapy volume delineation in non-small-cell lung cancer. Int J Radiat Oncol Biol Phys. 2004;59:78–86.
3. Bradley JD, Perez CA, Dehdashti F, Siegel BA. Implementing biologic target volumes in radiation treatment planning for non-small cell lung cancer. J Nucl Med. 2004;45 Suppl 1:96S–101.
4. Bradley J. Applications for FDG-PET in lung cancer; staging, targeting, and follow-up. Chicago: The Radiological Society of North America; 2004.
5. Erdi YE, Macapinlac H, Rosenzweig KE, Humm JL, Larson SM, Erdi AK, et al. Use of PET to monitor the response of lung cancer to radiation treatment. Eur J Nucl Med. 2000;27:861–6.

6. Mac Manus MP, Hicks RJ. PET scanning in lung cancer: current status and future directions. Semin Surg Oncol. 2003;21:149–55.

7. Mac Manus MP, Hicks RJ, Matthews JP, McKenzie A, Rischin D, Salminen EK, et al. Positron emission tomography is superior to computed tomography scanning for response-assessment after radical radiotherapy or chemoradiotherapy in patients with non-small-cell lung cancer. J Clin Oncol. 2003;21:1285–92.

8. MacManus MR, Hicks R, Fisher R, Rischin D, Michael M, Wirth A, et al. FDG-PET-detected extracranial metastasis in patients with non-small cell lung cancer undergoing staging for surgery or radical radiotherapy – survival correlates with metastatic disease burden. Acta Oncol. 2003;42:48–54.

9. Pandit N, Gonen M, Krug L, Larson SM. Prognostic value of [18F]FDG-PET imaging in small cell lung cancer. Eur J Nucl Med Mol Imaging. 2003;30:78–84.

10. Toloza EM, Harpole L, McCrory DC. Noninvasive staging of non-small cell lung cancer: a review of the current evidence. Chest. 2003;123:137S–46.

11. Schwartz DL, Ford E, Rajendran J, Yueh B, Coltrera MD, Virgin J, et al. FDG-PET/CT imaging for preradiotherapy staging of head-and-neck squamous cell carcinoma. Int J Radiat Oncol Biol Phys. 2005;61:129–36.

12. Suarez Fernandez JP, Maldonado Suarez A, Dominguez Grande ML, Santos Ortega M, Rodriguez Villalba S, Garcia Camanaque L, et al. Positron emission tomography (PET) imaging in head and neck cancer. Acta Otorrinolaringol Esp. 2004;55:303–9.

13. Oyama N, Miller TR, Dehdashti F, Siegel BA, Fischer KC, Michalski JM, et al. 11C-acetate PET imaging of prostate cancer: detection of recurrent disease at PSA relapse. J Nucl Med. 2003;44:549–55.

14. Mutic S, Malyapa RS, Grigsby PW, Dehdashti F, Miller TR, Zoberi I, et al. PET-guided IMRT for cervical carcinoma with positive para-aortic lymph nodes-a dose-escalation treatment planning study. Int J Radiat Oncol Biol Phys. 2003;55:28–35.

15. Miller TR, Grigsby PW. Measurement of tumor volume by PET to evaluate prognosis in patients with advanced cervical cancer treated by radiation therapy. Int J Radiat Oncol Biol Phys. 2002;53:353–9.

16. Ciernik IF. Radiotherapy of rectal cancer. Schweiz Rundsch Med Prax. 2004;93:1441–6.

17. Castellucci P, Zinzani P, Nanni C, Farsad M, Moretti A, Alinari L, et al. 18F-FDG PET early after radiotherapy in lymphoma patients. Cancer Biother Radiopharm. 2004;19:606–12.

18. Spaepen K, Stroobants S, Verhoef G, Mortelmans L. Positron emission tomography with [(18)F]FDG for therapy response monitoring in lymphoma patients. Eur J Nucl Med Mol Imaging. 2003;30 Suppl 1:S97–105.

19. Fogarty GB, Tartaglia CJ, Peters LJ. Primary melanoma of the oesophagus well palliated by radiotherapy. Br J Radiol. 2004;77:1050–2.

20. Biersack HJ, Bender H, Palmedo H. FDG-PET in monitoring therapy of breast cancer. Eur J Nucl Med Mol Imaging. 2004;31 Suppl 1:S112–7.

21. Lind P, Igerc I, Beyer T, Reinprecht P, Hausegger K. Advantages and limitations of FDG PET in the follow-up of breast cancer. Eur J Nucl Med Mol Imaging. 2004;31 Suppl 1:S125–34.

22. Zangheri B, Messa C, Picchio M, Gianolli L, Landoni C, Fazio F. PET/CT and breast cancer. Eur J Nucl Med Mol Imaging. 2004;31 Suppl 1:S135–42.

23. Brun E, Kjellen E, Tennvall J, Ohlsson T, Sandell A, Perfekt R, et al. FDG PET studies during treatment: prediction of therapy outcome in head and neck squamous cell carcinoma. Head Neck. 2002;24:127–35.

24. Hope AJ, Saha P, Grigsby PW. FDG-PET in carcinoma of the uterine cervix with endometrial extension. Cancer. 2006;106:196–200.

25. Kalff V, Duong C, Drummond EG, Matthews JP, Hicks RJ. Findings on 18F-FDG PET scans after neoadjuvant chemoradiation provides prognostic stratification in patients with locally advanced rectal carcinoma subsequently treated by radical surgery. J Nucl Med. 2006;47:14–22.

26. Hicks RJ, Mac Manus MP, Matthews JP, Hogg A, Binns D, Rischin D, et al. Early FDG-PET imaging after radical radiotherapy for non-small-cell lung cancer: inflammatory changes in normal tissues correlate with tumor response and do not confound therapeutic response evaluation. Int J Radiat Oncol Biol Phys. 2004;60:412–8.

27. Grigsby PW, Siegel BA, Dehdashti F, Rader J, Zoberi I. Posttherapy [18F] fluorodeoxyglucose positron emission tomography in carcinoma of the cervix: response and outcome. J Clin Oncol. 2004;22:2167–71.

28. Shields AF. Positron emission tomography measurement of tumor metabolism and growth: its expanding role in oncology. Mol Imaging Biol. 2006;8:141–50.

29. Denecke T, Rau B, Hoffmann KT, Hildebrandt B, Ruf J, Gutberlet M, et al. Comparison of CT, MRI and FDG-PET in response prediction of patients with locally advanced rectal cancer after multimodal preoperative therapy: is there a benefit in using functional imaging? Eur Radiol. 2005;15:1658–66.

30. Benz MR, Allen-Auerbach MS, Eilber FC, Chen HJJ, Dry S, Phelps ME, et al. Combined assessment of metabolic and volumetric changes for assessment of tumor response in patients with soft-tissue sarcomas. J Nucl Med. 2008;49:1579–84. doi:10.2967/jnumed.108.053694.

31. Yang D-H, Min J-J, Jeong Y, Ahn J-S, Kim Y-K, Cho S-H, et al. The combined evaluation of interim contrast-enhanced computerized tomography (CT)

and FDG-PET/CT predicts the clinical outcomes and may impact on the therapeutic plans in patients with aggressive non-Hodgkin's lymphoma. Ann Hematol. 2009;88:425–32.

32. Lambin P, Rios-Velazquez E, Leijenaar R, Carvalho S, van Stiphout RG, Granton P, et al. Radiomics: extracting more information from medical images using advanced feature analysis. Eur J Cancer. 2012; 48:441–6.doi:10.1016/j.ejca.2011.11.036.doi:S0959-8049(11)00999-3 [pii].

33. Kumar V, Gu Y, Basu S, Berglund A, Eschrich SA, Schabath MB, et al. Radiomics: the process and the challenges. Magn Reson Imaging. 2012;30:1234–48. doi:10.1016/j.mri.2012.06.010. doi:S0730-725X(12)00220-2 [pii].

34. El Naqa I, Grigsby P, Apte A, Kidd E, Donnelly E, Khullar D, et al. Exploring feature-based approaches in PET images for predicting cancer treatment outcomes. Pattern Recognit. 2009;42:1162–71. doi:10.1016/j.patcog.2008.08.011.

35. Kidd EA, El Naqa I, Siegel BA, Dehdashti F, Grigsby PW. FDG-PET-based prognostic nomograms for locally advanced cervical cancer. Gynecol Oncol. 2012;127:136–40. doi:10.1016/j.ygyno.2012.06.027. doi:S0090-8258(12)00478-7 [pii].

36. Vaidya M, Creach KM, Frye J, Dehdashti F, Bradley JD, El Naqa I. Combined PET/CT image characteristics for radiotherapy tumor response in lung cancer. Radiother Oncol. 2012;102:239–45. doi:10.1016/j.radonc.2011.10.014. doi:S0167-8140(11)00626-8 [pii].

37. El Naqa I. The role of quantitative PET in predicting cancer treatment outcomes. Clin Transl Imaging. 2014;2:305–20. doi:10.1007/s40336-014-0063-1.

38. Strauss LG, Conti PS. The applications of PET in clinical oncology. J Nucl Med. 1991;32:623–48.

39. Larson SM, Erdi Y, Akhurst T, Mazumdar M, Macapinlac HA, Finn RD, et al. Tumor treatment response based on visual and quantitative changes in global tumor glycolysis using PET-FDG imaging. The visual response score and the change in total lesion glycolysis. Clin Positron Imaging. 1999;2:159–71. doi:S1095039799000163 [pii].

40. Jain AK. Fundamentals of digital image processing. Englewood Cliffs: Prentice Hall; 1989.

41. O'Sullivan F, Roy S, O'Sullivan J, Vernon C, Eary J. Incorporation of tumor shape into an assessment of spatial heterogeneity for human sarcomas imaged with FDG-PET. Biostatistics. 2005;6:293–301. doi:10.1093/biostatistics/kxi010.

42. O'Sullivan F, Roy S, Eary J. A statistical measure of tissue heterogeneity with application to 3D PET sarcoma data. Biostatistics. 2003;4:433–48. doi:10.1093/biostatistics/4.3.433.

43. Castleman KR. Digital image processing. Englewood Cliffs: Prentice Hall; 1996.

44. Haralick R, Shanmugam K, Dinstein I. Texture features for image classification. IEEE Trans Sys Man Cyb SMC. 1973;3:610–21.

45. Zhang J, Tan T. Brief review of invariant texture analysis methods. Pattern Recognit. 2002;35:735–47. doi:http://dx.doi.org/10.1016/S0031-3203(01)00074-7.

46. Castellano G, Bonilha L, Li LM, Cendes F. Texture analysis of medical images. Clin Radiol. 2004;59:1061–9. doi:http://dx.doi.org/10.1016/j.crad.2004.07.008.

47. Chicklore S, Goh V, Siddique M, Roy A, Marsden P, Cook GR. Quantifying tumour heterogeneity in 18F-FDG PET/CT imaging by texture analysis. Eur J Nucl Med Mol Imaging. 2013;40:133–40. doi:10.1007/s00259-012-2247-0.

48. Tixier F, Le Rest CC, Hatt M, Albarghach N, Pradier O, Metges J-P, et al. Intratumor heterogeneity characterized by textural features on baseline 18F-FDG PET images predicts response to concomitant radiochemotherapy in esophageal cancer. J Nucl Med. 2011;52:369–78. doi:10.2967/jnumed.110.082404.

49. Cheng N-M, Dean Fang Y-H, Tung-Chieh Chang J, Huang C-G, Tsan D-L, Ng S-H, et al. Textural features of pretreatment 18F-FDG PET/CT images: prognostic significance in patients with advanced T-stage oropharyngeal squamous cell carcinoma. J Nucl Med. 2013;54:1703–9. doi:10.2967/jnumed.112.119289.

50. Cook GJR, Yip C, Siddique M, Goh V, Chicklore S, Roy A, et al. Are pretreatment 18F-FDG PET tumor textural features in non–small cell lung cancer associated with response and survival after chemoradiotherapy? J Nucl Med. 2013;54:19–26. doi:10.2967/jnumed.112.107375.

51. Szczypinski PM, Strzelecki M, Materka A, Klepaczko A. MaZda – a software package for image texture analysis. Comput Methods Programs Biomed. 2009;94:66–76. doi:10.1016/j.cmpb.2008.08.005.

52. Watabe H, Ikoma Y, Kimura Y, Naganawa M, Shidahara M. PET kinetic analysis – compartmental model. Ann Nucl Med. 2006;20:583–8.

53. Graham MM, Peterson LM, Hayward RM. Comparison of simplified quantitative analyses of FDG uptake. Nucl Med Biol. 2000;27:647–55.

54. Patlak CS, Blasberg RG. Graphical evaluation of blood-to-brain transfer constants from multiple-time uptake data. Generalizations. J Cereb Blood Flow Metab. 1985;5:584–90.

55. Choi NC, Fischman AJ, Niemierko A, Ryu JS, Lynch T, Wain J, et al. Dose–response relationship between probability of pathologic tumor control and glucose metabolic rate measured with FDG PET after preoperative chemoradiotherapy in locally advanced non-small-cell lung cancer. Int J Radiat Oncol Biol Phys. 2002;54:1024–35. doi:S0360301602030389 [pii].

56. Thorwarth D, Eschmann S-M, Holzner F, Paulsen F, Alber M. Combined uptake of [18F]FDG and [18F]FMISO correlates with radiation therapy outcome in head-and-neck cancer patients. Radiother Oncol. 2006;80:151–6.

57. Thorwarth D, Eschmann S-M, Paulsen F, Alber M. A model of reoxygenation dynamics of head-and-neck tumors based on serial 18F-fluoromisonidazole positron emission tomography investigations. Int J Radiat Oncol Biol Phys. 2007;68:515–21.

58. Turkheimer FE, Aston JA, Asselin MC, Hinz R. Multi-resolution Bayesian regression in PET dynamic studies using wavelets. Neuroimage. 2006; 32:111–21. doi:10.1016/j.neuroimage.2006.03.002. doi:S1053-8119(06)00180-7 [pii].

59. Milker-Zabel S, Zabel-du Bois A, Henze M, Huber P, Schulz-Ertner D, Hoess A, et al. Improved target volume definition for fractionated stereotactic radiotherapy in patients with intracranial meningiomas by correlation of CT, MRI, and [68Ga]-DOTATOC-PET. Int J Radiat Oncol Biol Phys. 2006;65:222–7.

60. Tofts PS, Brix G, Buckley DL, Evelhoch JL, Henderson E, Knopp MV, et al. Estimating kinetic parameters from dynamic contrast-enhanced T(1)-weighted MRI of a diffusable tracer: standardized quantities and symbols. J Magn Reson Imaging. 1999;10:223–32. doi:10.1002/(SICI)1522-2586(199909) 10:3<223::AID-JMRI2>3.0.CO;2-S [pii].

61. Hajnal JV, Hawkes DJ, Hill DLG. Medical image registration. Boca Raton: CRC Press; 2001.

62. Yang D, Zheng J, Nofal A, Wu Y, Deasy J, El Naqa I. Techniques and software tool for 3D multimodality medical image segmentation Journal of radiation oncology informatics. 2009:accepted.

63. Yang D, Brame S, El Naqa I, Aditya A, Wu Y, Goddu SM, et al. Technical note: DIRART – a software suite for deformable image registration and adaptive radiotherapy research. Med Phys. 2011;38: 67–77.

64. Pham DL, Xu C, Prince JL. Current methods in medical image segmentation. Annu Rev Biomed Eng. 2000;2:315–37.

65. Suri JS, Setarehdan SK, Singh S. Advanced algorithmic approaches to medical image segmentation: state-of-the-art applications in cardiology, neurology, mammography, and pathology. New York: Springer; 2002.

66. Zaidi H, Abdoli M, Fuentes CL, El Naqa IM. Comparative methods for PET image segmentation in pharyngolaryngeal squamous cell carcinoma. Eur J Nucl Med Mol Imaging. 2012;39(5):881–91. doi:10.1007/s00259-011-2053-0.

67. Zaidi H, El Naqa I. PET-guided delineation of radiation therapy treatment volumes: a survey of image segmentation techniques. Eur J Nucl Med Mol Imaging. 2010;37:2165–87. doi:10.1007/s00259-010-1423-3.

68. Yoo TS, Ackerman MJ, Lorensen WE, Schroeder W, Chalana V, Aylward S, et al. Engineering and algorithm design for an image processing API: a technical report on ITK – the insight toolkit. In: Proceedings of medicine meets virtual reality. 2002;586–92.

69. Papademetris X, Jackowski M, Rajeevan N, Constable RT, Staib L. BioImage suite: an integrated medical image analysis suite. Insight J. 2005; 2006:209.

70. McAuliffe MJ, Lalonde FM, McGarry D, Gandler W, Csaky K, Trus BL. Medical image processing, analysis & visualization in clinical research. In: Proceedings of the fourteenth IEEE symposium on computer-based medical systems. IEEE Computer Society. 2001.

71. Abramoff MD, Magelhaes PJ, Ram SJ. Image processing with imageJ. Biophotonics Int. 2004;11:36–42.

72. Fedorov A, Beichel R, Kalpathy-Cramer J, Finet J, Fillion-Robin JC, Pujol S, et al. 3D Slicer as an image computing platform for the quantitative imaging network. Magn Reson Imaging. 2012;30:1323–41. doi:10.1016/j.mri.2012.05.001.

73. El Naqa I, Yang D, Apte A, Khullar D, Mutic S, Zheng J, et al. Concurrent multimodality image segmentation by active contours for radiotherapy treatment planning. Med Phys. 2007;34:4738–49.

74. Sebbahi A, Herment A, de Cesare A, Mousseaux E. Multimodality cardiovascular image segmentation using a deformable contour model. Comput Med Imaging Graph. 1997;21:79–89.

75. Zheng J, Naqa IE, Rowold FE, Pilgram TK, Woodard PK, Saffitz JE, et al. Quantitative assessment of coronary artery plaque vulnerability by high-resolution magnetic resonance imaging and computational biomechanics: a pilot study ex vivo. Magn Reson Med. 2005;54:1360–8.

76. Sethian JA. Level set methods and fast marching methods: evolving interfaces in computational geometry, fluid mechanics, computer vision, and material science. 2nd ed. Cambridge: Cambridge University Press; 1999.

77. Xu C, Pham DL, Prince JL. Image segmentation using deformable models. In: Sonka M, Fitzpatrick JM, editors. Handbook of medical imaging: medical image processing and analysis. Bellingham: SPIE (The International Society for Optical Engineering) Press; 2002. p. 129–74.

78. Suri JS, Kecheng L, Singh S, Laxminarayan SN, Xiaolan Z, Reden L. Shape recovery algorithms using level sets in 2-D/3-D medical imagery: a state-of-the-art review. IEEE Trans Inf Technol Biomed. 2002;6:8–28.

79. Aubert G. Mathematical problems in image processing: partial differential equations and the calculus of variations. 2nd ed. New York: Springer; 2006.

80. Osher S, Fedkiw RP. Level set methods and dynamic implicit surfaces. New York: Springer; 2003.

81. Kass M, Witkin A, Terzopoulos. Snakes: active contour models. In: First international conference on computer vision, London. 1987;259–68.

82. El Naqa I, Low DA, Bradley JD, Vicic M, Deasy JO. Deblurring of breathing motion artifacts in thoracic PET images by deconvolution methods. Med Phys. 2006;33:3587–600.

83. Wong CY, Schmidt J, Bong JS, Chundru S, Kestin L, Yan D, et al. Correlating metabolic and anatomic

responses of primary lung cancers to radiotherapy by combined F-18 FDG PET-CT imaging. Radiat Oncol. 2007;2:18. doi:10.1186/1748-717X-2-18. doi:1748-717X-2-18 [pii].

84. Coon D, Gokhale AS, Burton SA, Heron DE, Ozhasoglu C, Christie N. Fractionated stereotactic body radiation therapy in the treatment of primary, recurrent, and metastatic lung tumors: the role of positron emission tomography/computed tomography-based treatment planning. Clin Lung Cancer. 2008;9:217–21. doi:10.3816/CLC.2008.n.032. doi:935437162W233526 [pii].

85. Steel GG. Basic clinical radiobiology. 3rd ed. London/New York/Arnold: Oxford University Press; 2002.

86. Webb S. The physics of three-dimensional radiation therapy: conformal radiotherapy, radiosurgery, and treatment planning. Bristol/Philadelphia: Institute of Physics Pub; 2001.

87. El Naqa I. Outcomes modeling. In: Starkschall G, Siochi C, editors. Informatics in radiation oncology. Boca Raton: CRC Press/Taylor and Francis; 2013. p. 257–75.

88. El Naqa I, Suneja G, Lindsay PE, Hope AJ, Alaly JR, Vicic M, et al. Dose response explorer: an integrated open-source tool for exploring and modelling radiotherapy dose-volume outcome relationships. Phys Med Biol. 2006;51:5719–35.

89. El-Naqa I, Yang Y, Galatsanos NP, Nishikawa RM, Wernick MN. A similarity learning approach to content-based image retrieval: application to digital mammography. IEEE Trans Med Imaging. 2004;23:1233–44. doi:10.1109/TMI.2004.834601.

90. Deasy JO, El Naqa I. Image-based modeling of normal tissue complication probability for radiation therapy. In: Mehta M, Bentzen S, editors. Radiation oncology advances. New York: Springer; 2007.

91. El Naqa I, Bradley JD, Lindsay PE, Blanco AI, Vicic M, Hope AJ, et al. Multi-variable modeling of radiotherapy outcomes including dose-volume and clinical factors. Int J Radiat Oncol Biol Phys. 2006;64:1275–86.

92. Moses WW. Fundamental limits of spatial resolution in PET. Nucl Instrum Meth Phys Res A Accelerators Spectrometers Detectors Assoc Equipment. 2011;648 Suppl 1:S236–40. doi:10.1016/j.nima.2010.11.092.

93. Tong S, Alessio AM, Kinahan PE. Image reconstruction for PET/CT scanners: past achievements and future challenges. Imaging Med. 2010;2:529–45. doi:10.2217/iim.10.49.

94. Nahmias C, Wahl LM. Reproducibility of standardized uptake value measurements determined by 18F-FDG PET in malignant tumors. J Nucl Med. 2008;49:1804–8. doi:10.2967/jnumed.108.054239.

95. Kinahan PE, Fletcher JW. Positron emission tomography-computed tomography standardized uptake values in clinical practice and assessing response to therapy. Semi Ultrasound CT MRI.

2010;31:496–505. doi:http://dx.doi.org/10.1053/j.sult.2010.10.001.

96. Hatt M, Cheze-Le Rest C, Aboagye EO, Kenny LM, Rosso L, Turkheimer FE, et al. Reproducibility of 18F-FDG and 3′-deoxy-3′-18F-fluorothymidine PET tumor volume measurements. J Nucl Med. 2010;51:1368–76. doi:10.2967/jnumed.110.078501.

97. Galavis PE, Hollensen C, Jallow N, Paliwal B, Jeraj R. Variability of textural features in FDG PET images due to different acquisition modes and reconstruction parameters. Acta Oncol. 2010;49:1012–6. doi:10.3109/0284186X.2010.498437.

98. Cheng NM, Fang YH, Yen TC. The promise and limits of PET texture analysis. Ann Nucl Med. 2013;27:867–9. doi:10.1007/s12149-013-0759-8.

99. Tixier F, Hatt M, Le Rest CC, Le Pogam A, Corcos L, Visvikis D. Reproducibility of tumor uptake heterogeneity characterization through textural feature analysis in 18F-FDG PET. J Nucl Med. 2012;53:693–700. doi:10.2967/jnumed.111.099127.

100. El Naqa I, Kawrakow I, Fippel M, Siebers JV, Lindsay PE, Wickerhauser MV, et al. A comparison of Monte Carlo dose calculation denoising techniques. Phys Med Biol. 2005;50:909–22. doi:10.1088/0031-9155/50/5/014. doi:S0031-9155(05)86128-7 [pii].

101. Le Pogam A, Hanzouli H, Hatt M, Cheze Le Rest C, Visvikis D. Denoising of PET images by combining wavelets and curvelets for improved preservation of resolution and quantitation. Med Image Anal. 2013;17:877–91. doi:10.1016/j.media.2013.05.005.

102. El Naqa I, Li R, Murphy MJ, editors. Machine learning in radiation oncology: theory and application. 1st ed. Cham: Springer International Publishing; 2015.

103. El Naqa I, Bradley J, Deasy J. Machine learning methods for radiobiological outcome modeling. In: Mehta M, Paliwal B, Bentzen S, editors. Physical, chemical, and biological targeting in radiation oncology. Madison: Medical Physics Publishing; 2005.

104. El-Naqa I, Yang Y, Galatsanos NP, Nishikawa RM, Wernick MN. A similarity learning approach to content-based image retrieval: application to digital mammography. IEEE Trans Med Imaging. 2004;23:1233–44.

105. El-Naqa I, Yang Y, Wernick MN, Galatsanos NP, Nishikawa RM. A support vector machine approach for detection of microcalcifications. IEEE Trans Med Imaging. 2002;21:1552–63.

106. Schèolkopf B, Tsuda K, Vert J-P. Kernel methods in computational biology. Cambridge, MA: MIT Press; 2004.

107. Shawe-Taylor J, Cristianini N. Kernel methods for pattern analysis. Cambridge/New York: Cambridge University Press; 2004.

108. Hastie T, Tibshirani R, Friedman JH. The elements of statistical learning: data mining, inference, and prediction: with 200 full-color illustrations. New York: Springer; 2001.